Dynamic Black-hole Emission Tomography with Physics-informed Neural Fields

Supplementary Material

A. Velocity mismatch ablation

We performed an ablation study of the error in the assumed velocity model v^i_{prior}. Fig. 10 shows emissivity reconstruction results when assuming different velocity priors with varying amounts of mismatch. The ground-truth velocity follows the AART model with $\xi = 0.7$ and $\beta = \beta_r = \beta_\phi = 0.9$. We ran optimizations for the following scenarios:

- Correct velocity: $\xi_{\text{prior}} = 0.7$, $\beta_{\text{prior}} = 0.9$
- Slight mismatch in β: $\xi_{\text{prior}} = 0.7$, $\beta = 1.0$
- Large mismatch in β: $\xi_{\text{prior}} = 0.7$, $\beta = 0.2$
- Slight mismatch in ξ: $\xi_{\text{prior}} = 1.0$, $\beta = 0.9$
- Large mismatch in ξ: $\xi_{\text{prior}} = 0.2$, $\beta = 0.9$

A slight mismatch does not notably degrade reconstruction, and even a large mismatch still leads to a decent reconstruction. These results indicate that our method is robust to errors in the assumed velocity model. The main reason is that velocity regularization guides the emissivity and velocity reconstructions at the beginning of optimization, but as we gradually decrease the regularization strength, the reconstruction is mostly informed by the measurements.

B. Implementation details

Here we provide implementation details in addition to those provided in Sec. 5.1.

Simulating emissivity fields To create ground-truth emissivity fields, we introduced $N_{\text{flare}} = 20$ "flares" at evenly-spaced intervals from time $t = 12.5$ to $t = 13.5$ hours (UTC). Each flare consisted of 1, 2, or 3 (sampled uniformly) hotspots. We randomly sampled hotspots with $r_{\min} = 7$ and $r_{\max} = 8$ and $\sigma_{\min} = 0.5$ and $\sigma_{\max} = 1.0$. We propagated the hotspots according to the AART velocity model with $\xi = 0.7$ and $\beta = \beta_r = \beta_\phi = 0.9$.

Simulating EHT measurements We used the `eht-imaging` library to simulate time-varying EHT measurements of the ground-truth emissivity fields. Sec. B.1 lists the parameter values used for simulating the EHT observation. The observation time window of 12.5 to 13.5 hours (UTC) was chosen because 12.5 to 14.2 is considered a good observation time for Sgr A*. We set the pixel size (psize) parameter based on a field of view of 25 M (about 125.345 μas) and 100 pixels in each direction in the image.

Network architecture We used MLPs with 4 layers with ReLU activations. Each layer was 256 units wide in the emissivity network and 128 units wide in the velocity network. We set the position-encoding degree as $L = 3$ for the emissivity network and $L = 1$ for the velocity network. The emissivity 4D MLP and velocity MLP had 212,225 and 50,819 parameters, respectively.

B.1. Optimization settings

Hyperparameters We set $\lambda_{\text{data}} = 1$ and $\Delta t = 0.01$ for all measurement settings. As mentioned in Sec. 5.1, we gradually decreased the velocity regularization weight from λ_{init} to λ_{final}. When fitting to EHT measurements with negligible noise, we set $\lambda_{\text{dyn}} = 10^5$ and $\lambda_{\text{init}} = 10^6, \lambda_{\text{final}} = 10$. When fitting to EHT measurements with realistic Gaussian noise, we set $\lambda_{\text{dyn}} = 10$ and $\lambda_{\text{init}} = 100, \lambda_{\text{final}} = 10^{-4}$. When fitting to full images, we set $\lambda_{\text{dyn}} = 0.1$ and $\lambda_{\text{init}} = 1, \lambda_{\text{final}} = 10^{-6}$.

Runtime On 1 NVIDIA A100 80GB GPU with simulated ngEHT data, it took 28 hours to run 100K optimization steps with a batch size of 6. A "batch" refers to the number of time frames used to compute the data-fit loss, defined in Eq. (9), which takes an expectation over the measurement time frames, and the dynamics loss, defined in Eq. (10), which takes an expectation over the time interval $[0, T]$.

ODE solver To solve the integral in Eq. (12), we used the Tsitouras 5/4 solver [44] implemented in Diffrax [24] with a constant step size of 0.001.

C. EHT measurements

Here we provide details on very-long-baseline-interferometry (VLBI), which is the technique that the EHT uses to obtain Fourier measurements of the sky's image. We denote the image by $I(x, y)$, where (x, y) are 2D image coordinates. The van Cittert-Zernike Theorem [45, 48] states that the ideal visibility v^*_{ij} measured

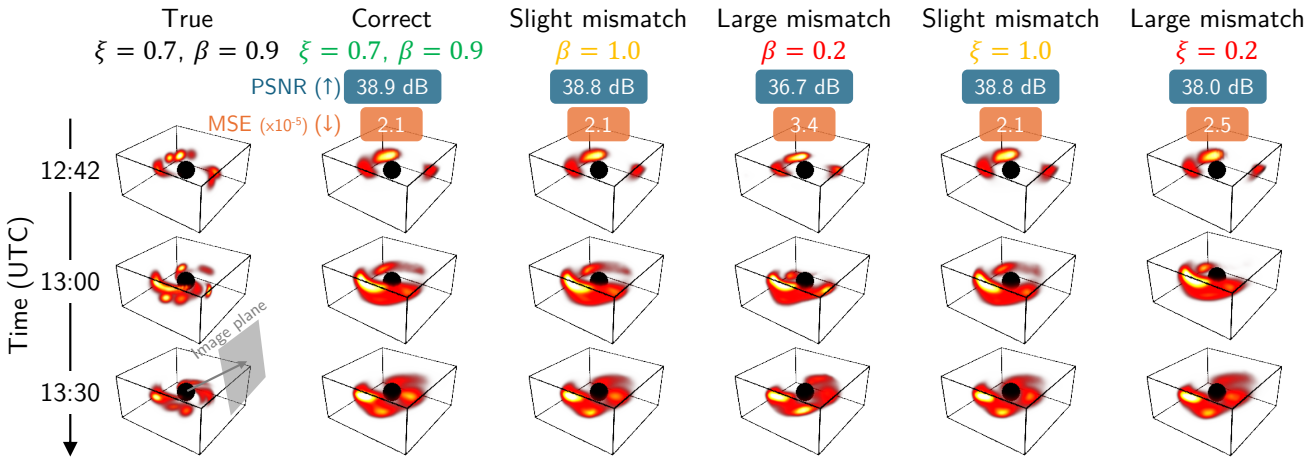

Figure 10. Ablation of the amount of mismatch in the velocity prior used for velocity regularization.

Parameter	Value
ra	17.761120
dec	−29.007797
rf	230×10^9
bw	2×10^9
mjd	60775 (10/04/2025)
source	SgrA
tstart	12.5
tstop	13.5
tint	102
tadv	102
tau	0.1
taup	0.1
polrep_obs	stokes
elevmin	10.0
elevmax	85.0

Table 2. EHT measurement parameters.

by the baseline $\boldsymbol{b}_{ij}$ between telescopes i and j is a single (u, v) measurement on the complex 2D Fourier plane [41]:

$$v_{ij}^* := \tilde{I}(u,v) = \int\int I(x,y) e^{-2\pi \mathrm{i}(xu+yv)} \mathrm{d}x\mathrm{d}y. \quad (15)$$

An array of N_s telescopes has $\binom{N_s}{2}$ independent baselines, each providing a visibility at each point in time.

In practice, there are multiple sources of noise in the measured visibilities. Baseline-dependent **thermal noise** is modeled as a Gaussian random variable $\varepsilon_{ij} \sim \mathcal{N}(0, \sigma_{ij}^2)$, where σ_{ij} is based on the system equivalent flux density (SEFD) of each telescope: $\sigma_{ij} \propto \sqrt{\mathrm{SEFD}_i + \mathrm{SEFD}_j}$. The **station-dependent gain error** g_i arises from each telescope i using its own time-dependent 2×2 Jones matrix [17]. The **station-dependent phase error** ϕ_i arises from atmospheric turbulence that causes light to travel at different velocities toward each telescope [18, 25, 40]. Other sources of corruption, including polarization leakage and bandpass errors, may introduce baseline-dependent errors, but they are slow-varying and assumed to be removable with *a priori* calibration [6]. The measured visibility of baseline $\boldsymbol{b}_{ij}$ can be written as

$$v_{ij} = g_i g_j e^{\mathrm{i}(\phi_i - \phi_j)} v_{ij}^* + \varepsilon_{ij}. \quad (16)$$

C.1. Closure phases

It is possible to deal with station-dependent errors by using *closure quantities* – specifically closure phases and closure amplitudes – that are robust to such errors. In Sec. 5.7 we overcome atmospheric noise by using closure phases [21], which are formed by multiplying the three baselines within each triangle of telescopes i, j, k:

$$\begin{aligned} v_{ij} v_{jk} v_{ki} = &\left(g_i g_j e^{\mathrm{i}(\phi_i - \phi_j)} v_{ij}^* + \varepsilon_{ij}\right) \\ &\left(g_j g_k e^{\mathrm{i}(\phi_j - \phi_k)} v_{jk}^* + \varepsilon_{jk}\right) \\ &\left(g_k g_i e^{\mathrm{i}(\phi_k - \phi_j)} v_{ki}^* + \varepsilon_{ki}\right) \quad (17) \\ =& g_{ijk}^2 e^{\mathrm{i}(\phi_i - \phi_j)} e^{\mathrm{i}(\phi_j - \phi_k)} e^{\mathrm{i}(\phi_k - \phi_i)} v_{ij}^* v_{jk}^* v_{ki}^* + \varepsilon_{ijk} \quad (18) \\ =& g_{ijk}^2 v_{ij}^* v_{jk}^* v_{ki}^* + \varepsilon_{ijk}, \quad (19) \end{aligned}$$

where ε_{ijk} is a Gaussian random variable. Although there are $\binom{N_s}{3}$ possible triplets in a telescope array, there are $\binom{N_s-1}{2}$ linearly independent closure phases.

D. Details about black-hole emission physics

Here we provide more detailed formulae for the quantities that we use to model fluid velocity and radiative transfer near black holes. A mathematical object known as a *spacetime metric* captures the geometry of the warped spacetime

around a black hole. It is represented as a *metric tensor* $g_{\mu\nu}$, which allows us to define distances between points in spacetime, which are denoted by x^μ.

Preliminaries In general relativity, we work with *contravariant* (index-up) vectors a^μ and *covariant* (index-down) vectors a_μ. To lower indices, we multiply a contravariant vector by the spacetime metric:

$$a_\mu = g_{\mu\nu} a^\nu. \tag{20}$$

Conversely, to raise indices, we multiply a covariant vector by the inverse metric:

$$b^\mu = g^{\mu\nu} b_\nu. \tag{21}$$

Here $\mu, \nu \in (0, 1, 2, 3)$ are indices. We can compute dot products between pairs of covariant and contravariant vectors:

$$a \cdot b = a^\mu b_\mu = a_\mu b^\mu = \sum_{i=0}^{3} a_i b^i. \tag{22}$$

D.1. Converting from the four-velocity

Recall from Sec. 3.1.1 that we denote the three-velocity vector by

$$v^i = \left(v^r, v^\theta, v^\phi\right) = \left(\frac{\mathrm{d}r}{\mathrm{d}t}, \frac{\mathrm{d}\theta}{\mathrm{d}t}, \frac{\mathrm{d}\phi}{\mathrm{d}t}\right) \tag{23}$$

and the four-velocity vector by

$$u^\mu = \left(\frac{\mathrm{d}t}{\mathrm{d}\tau}, \frac{\mathrm{d}r}{\mathrm{d}\tau}, \frac{\mathrm{d}\theta}{\mathrm{d}\tau}, \frac{\mathrm{d}\phi}{\mathrm{d}\tau}\right) = u^t \left(1, v^r, v^\theta, v^\phi\right). \tag{24}$$

The four-velocity u^μ can be directly derived from v^i via Equation 24, with

$$u^t = \sqrt{\frac{-1}{g_{tt} + 2g_{ti}v^i + g_{ij}v^i v^j}} \tag{25}$$

to satisfy the normalization condition $u^\mu u_\mu = -1$.

D.2. Converting from the normal observer frame

As discussed in Sec. 3.1.2, we estimate velocities in the normal observer frame to avoid numerical instabilities. We denote the three-velocity in the normal observer frame by $\tilde{u}^i$. The conversion from $\tilde{u}^i$ to u^μ is given by

$$u^t = \frac{\gamma}{\alpha}, \tag{26}$$

$$u^i = \tilde{u}^i - \left(\frac{\gamma}{\alpha}\right)\beta^i, \tag{27}$$

where i is an index into (r, θ, ϕ). The lapse α and shift vector β^i are defined as

$$\alpha = \sqrt{\frac{1}{-g^{tt}}}, \tag{28}$$

$$\beta^i = -\frac{g^{ti}}{g^{tt}}. \tag{29}$$

The Lorentz factor $\gamma \geq 1$ can be computed from the normal-observer $\tilde{u}^i$ as

$$\gamma = \sqrt{1 + g_{ij}\tilde{u}^i\tilde{u}^j}. \tag{30}$$

The condition for the four-velocity to be physical is $\gamma > 1$. In Boyer-Lindquist coordinates in the Kerr spacetime, we have that

$$\gamma^2 = 1 + \frac{\Sigma}{\Delta}\left(u^r\right)^2 + \Sigma\left(u^\theta\right)^2 + \frac{\Xi \sin^2\theta}{\Sigma}\left(u^\phi\right)^2. \tag{31}$$

By inspection, we can see that $\gamma^2 > 1$ for all u^i. There may be numerical instabilities when $\Delta \to 0$, which happens at the horizon.

The conversion can be done in the other direction by solving for $\tilde{u}^i$ given u^μ in Equation 27. Recall that u^μ can be determined from v^i by computing u^t with Equation 25.

D.3. AART velocity model

Recall from Sec. 3.1.1 that we work with the AART velocity model Cárdenas-Avendaño et al. [9]. The model depends on a fixed spin a and mass M, and it is axially symmetric, meaning in the equatorial plane it only depends on the radius r. The AART model mixes two velocities: (1) a sub-Keplerian velocity denoted by u^μ_{subkep} and (2) an infall velocity denoted by u^μ_{infall}. The velocity u^μ_{subkep} is based on the Cunningham [8] model of Keplerian dynamics, which includes infall inside the innermost stable circular orbit (ISCO). The velocity u^μ_{infall} only represents infall due to geodesics, assuming a particle that starts with zero velocity at radius infinity. Here we provide formulae for u^μ_{subkep} and u^μ_{infall}, the derivations of which can be found in Appendix F of [5]. In the rest of this appendix, we will refer to the following common abbreviations in the Kerr metric:

$$\Delta = r^2 + a^2 - 2Mr, \tag{32}$$

$$\Sigma = r^2 + a^2\cos^2\theta, \tag{33}$$

$$\Xi = \left(r^2 + a^2\right)^2 - a^2\Delta\sin^2\theta, \tag{34}$$

$$\Omega = \frac{2Mar}{(r^2 + a^2)^2 - a^2\Delta\sin^2\theta}. \tag{35}$$

Sub-Keplerian velocity model The Cunningham model [8] treats the velocity differently depending on whether it is outside or inside the ISCO. The ISCO radius is given by

$$r_{\text{ISCO}} = M\left[3 + Z_2 \pm \sqrt{(3 - Z_1)(3 + Z_1 + 2Z_2)}\right], \tag{36}$$

where

$$Z_1 = 1 + (1 - a^2/M^2)^{1/3}\left[(1 + a/M)^{1/3} + (1 - a/M)^{1/3}\right], \tag{37}$$

$$Z_2 = \left(3a^2/M^2 + Z_1^2\right)^{1/2}. \tag{38}$$

We define the following quantities:

$$\lambda_r = \xi \cdot \frac{\text{sign}(a) \cdot s \cdot (r^2 + a^2 - 2s|a|\sqrt{r})}{r^{3/2} - 2\sqrt{r} + s|a|}, \tag{39}$$

$$\gamma_r = \sqrt{\frac{\Delta_r}{\Xi_r/r^2 - 4a\lambda_r/r - (1-2/r)\lambda_r^2}}, \tag{40}$$

where $\xi \in (0, 1]$ is a sub-Keplerianity parameter. Here $s = \pm 1$ signifies whether the orbit is in prograde ($s = 1$) or retrograde ($s = -1$). We define $\lambda^* = \lambda_{r_{\text{ISCO}}}$ and $\gamma^* = \gamma_{r_{\text{ISCO}}}$. The formulae for the four-velocity components depend on whether r is outside or inside the ISCO, with the main difference coming from negative radial velocity inside the ISCO. The components are computed as

$$u^t_{\text{subkep}}(r) = \begin{cases} \frac{\gamma_r}{\chi_r}, & r \geq r_{\text{ISCO}} \\ \frac{\gamma^*}{\chi^*_r}, & r \leq r_{\text{ISCO}} \end{cases}, \tag{41}$$

$$u^r_{\text{subkep}}(r) = \begin{cases} 0, & r \geq r_{\text{ISCO}} \\ -\frac{1}{r^2}\gamma^* \Delta_r \nu^*_r, & r < r_{\text{ISCO}} \end{cases}, \tag{42}$$

$$u^\theta_{\text{subkep}}(r) = 0 \tag{43}$$

$$u^\phi_{\text{subkep}}(r) = \begin{cases} u^t_{\text{subkep}}\Omega_r, & r \geq r_{\text{ISCO}} \\ u^t_{\text{subkep}}\Omega^*_r, & r < r_{\text{ISCO}} \end{cases}, \tag{44}$$

where we use the subscript r to denote a dependence on the radius r. Here

$$H_r = \frac{2r - a\lambda_r}{\Delta_r}, \tag{45}$$

$$\chi_r = \frac{1}{1 + \frac{2}{r}(1 + H_r)}, \tag{46}$$

and

$$H^*_r = \frac{2r - a\lambda^*}{\Delta_r}, \tag{47}$$

$$\chi^*_r = \frac{1}{1 + \frac{2}{r}(1 + H^*_r)}, \tag{48}$$

$$\nu^*_r = \frac{r}{\Delta_r}\sqrt{\frac{\Xi_r}{r^2} - \frac{4a\lambda^*}{r} - \left(1 - \frac{2}{r}\right)(\lambda^*)^2 - \frac{\Delta_r}{(\gamma^*)^2}}. \tag{49}$$

The azimuthal velocities are defined as

$$\Omega_r = \frac{\chi_r}{r^2}(\lambda_r + aH_r) \tag{50}$$

and

$$\Omega^*_r = \frac{\chi^*_r}{r^2}(\lambda^* + aH^*_r). \tag{51}$$

Infall velocity model The four-velocity components due to geodesic infall from infinity are given by

$$u^t_{\text{infall}}(r) = \frac{\Xi_r}{r^2\Delta_r}, \tag{52}$$

$$u^r_{\text{infall}}(r) = -\frac{\sqrt{2r(r^2 + a^2)}}{r^2}, \tag{53}$$

$$u^\theta_{\text{infall}}(r) = 0, \tag{54}$$

$$u^\phi_{\text{infall}}(r) = \frac{2a}{r\Delta_r}. \tag{55}$$

Putting everything together We define $\Omega_{\text{subkep}} = \frac{u^\phi_{\text{subkep}}(r)}{u^t_{\text{subkep}}(r)}$ and $\Omega_{\text{infall}} = \frac{u^\phi_{\text{infall}}(r)}{u^t_{\text{infall}}(r)}$. The four-velocity components of the general velocity model are given by

$$u^t(r) = \frac{1 + \frac{r^2(u^r)^2}{\Delta_r}}{1 - (r^2 + a^2)\Omega^2 - \frac{2}{r}(1 - a\Omega)^2}, \tag{56}$$

$$u^r(r) = \beta_r u^r_{\text{subkep}} + (1 - \beta_r)u^r_{\text{infall}}, \tag{57}$$

$$u^\theta(r) = 0, \tag{58}$$

$$u^\phi(r) = u^t(r) \cdot (\beta_\phi \Omega_{\text{subkep}} + (1 - \beta_\phi)\Omega_{\text{infall}}). \tag{59}$$

The parameters $\beta_\phi\, \beta_r \in [0, 1]$ determine the amount of influence of the sub-Keplerian model in the azimuthal and radial velocities, respectively.

D.4. Redshift

As mentioned in Sec. 3.1.3, there is a Doppler effect on the intensity of light that reaches the observer. The redshift factor depends on the velocity field. Assuming a photon energy of $E = 1$, the location-dependent redshift factor g is computed as

$$g = \frac{E}{-k_\mu u^\mu} = \frac{1}{-k_\mu u^\mu}, \tag{60}$$

where k_μ is the photon momentum vector. It is related to the derivative of the photon position $x^\mu(\tau)$ with respect to the Mino time τ:

$$\frac{\mathrm{d}x^\mu}{\mathrm{d}\tau} = \frac{\Sigma}{E}k^\mu = \Sigma k^\mu = \Sigma g^{\mu\nu}k_\nu \tag{61}$$

assuming $E = 1$. For a given spin and mass of the black hole, the photon momentum at every point in spacetime is fixed.